Journal of the Brazilian Society of Mechanical Sciences and Engineering (2023) 45:332
https://doi.org/10.1007/s40430-023-04245-3

TECHNICAL PAPER

Design method of enhancing the tightness of a spiral wound gasket with PTFE filling

Konrad Adamek[1] · **Przemysław Jaszak**[1]

Received: 21 November 2022 / Accepted: 5 May 2023 / Published online: 26 May 2023

Abstract

The paper presents the experimental research results and numerical computations of two constructions of a spiral wound gasket with a PTFE filling. The first construction was a standard one in which the shape of the spiral's windings in a cross section view resembles the shape of the letter 'V.' The second solution has an original, asymmetric shape of windings' profile. Based on the vast experimental research tests, it was proved that the gasket with an asymmetric shape of windings is characterized with larger stiffness than the standard design, as well as increased tightness. Numerical calculations and a topography analysis of the contact surface of the gaskets showed that the asymmetric gasket under load is characterized with a larger effective contact surface when compared to the standard gasket. The gasket of an asymmetric construction can have a special application at small contact stress, which allows to avoid an excessive stress of flanges and bolts.

Keywords Spiral wound gasket · Tightness improvement · Finite element method · PTFE

List of symbols

a	Arm of acting vertical force, m
A_G, A_V	Gasket surface, vertical surface of the coil's segment, m^2
d_i, d_e	Gasket diameter, internal, external, m
D, D_f	Fractal dimension of the pore and tortuous capillaries, respectively
f	Height of the vertical direction of the percolation channels, m
G	Roughness constant
F_V, F_H	Force, vertical, horizontal, N
E, E_U	Elastic modulus, modulus in plastic zone, MPa
h	Height of the gasket, m
K_V	Permeability, m^2
l, $l_{max,p}$	Length of the pore; characteristic and maximal, respectively, µm
n	Number of coils of the spiral windings
N	Numbers of pores
p	Contact pressure, MPa
R_e	Yield stress, MPa
r_i, r_e	Radius, internal, external, m
s	Length of vertical metal coil's segment, m
S, $S_{max,p}$	Cross section: gasket's profile, maximum of a pore, m^2
T	Torque, Nm
t_s, t_g	Thickness of metal tape, thickness of PTFE tape, m kg/s
X_i, Y_i,	Cartesian coordinates, m
y	Arm of acting vertical force, m
α	Angle, deg
λ, λ_{max}	Pore size; characteristic, maximal, µm
δ, $\delta_{max,p}$	Peak of the asperity and maximal of a pore, respectively, µm
σ_A, σ_R, σ_0, $\sigma_{(4\,h)}$	Gasket contact stress; assembly, residual, initial, final, MPa
τ	Capillary's tortuosity
ν	Poisson ratio

Abbreviations

SWG	Spiral wound gasket
FJ	Flange joint
PTFE	Polytetrafluoroethylene
EG	Expanded graphite

Technical Editor: João Marciano Laredo dos Reis.

✉ Konrad Adamek
konrad.adamek@pwr.edu.pl

Przemysław Jaszak
przemyslaw.jaszak@pwr.edu.pl

[1] Department of Mechanical and Power Engineering, Wroclaw University of Science and Technology, Wybrzeże Wyspiańskiego Street 27, 50-370 Wrocław, Poland

1 Introduction

A spiral wound gasket is one of the most common types of semimetal gaskets used in the flange-bolted joints of pressure installations. Such gaskets consist of spirally wound metal tape and filler material. A typical construction of a spiral wound gasket is presented in Fig. 1a. Generally, in the cross section view, the windings of both tapes after winding take the shape of the letter 'V' or 'W.' A spiral wound in such a way is usually fixed in metal distance rings, internal and/or external, which provide the gasket with larger stiffness, as well as protect the internal windings against so-called radial buckling [1–3]. The metal tape is usually made of materials, such as 304L, 316L, and monel. The tape of the filling material (depending on the sealing medium) is made of expanded graphite (EG) or polytetrafluoroethylene (PTFE).

The application of EG or PTFE depends mainly on the conditions the gasket is supposed to work in, i.e., the temperature used, pressure, and the kind of sealed medium. The biggest advantage of EG is the high tightness at a slight assembly stress, great resistance in higher and low temperatures [4], low fluid permeability [5], the low coefficient of the thermal expansion [6], and also the moderate degree of friction wear [7]. However, the disadvantages include high losses of mass while in contact with oxygen at elevated temperature, small elastic recovery, and a very low tensile strength [8]. In the case of PTFE, the advantages include high chemical resistance to aggressive media, resistance to electro-chemical corrosion, and higher (in comparison with EG) tensile strength [9]. The disadvantages, however, are the large thermal expansion, low value of the friction coefficient (which is a drawback since it may cause the so-called blowup effect), small tightness at a slight contact stress, and the big degree of creep and relaxation (even at room temperature). The high Poisson's ratio of PTFE causes a significant growth of the external and internal diameters of the gasket during compression. The lower ability of PTFE to plastic deformations in comparison with EG is an undesired feature, since at a low assembly stress, it leads to a lower degree of filling the irregularities of the sealing surfaces.

Throughout the years, many methods of improving the physical and chemical properties of PTFE have been proposed, which involved the modification of its structure. To increase its mechanical properties, especially improvement with regard to frictional wear, PTFE is filled with various additives, such as graphite flakes, what was the aim of the work presented in [10, 11], the combination of PTFE + 30(v)%Cu, PTFE + 30(v)%Cu2O, and PTFE + 30(v) % CuS composite [12–14]. The main purpose of this work was achieving the higher wear resistance of the external layer of the bearing. In order to enhance compressibility, expanded PTFE is applied.

Each of the abovementioned methods of enhancing the features of a material indispensably involves an increase in production costs. The paper focuses on a method of design to improve the tightness of a spiral wound gasket with PTFE filling without changing its structure. This method included the modification of the shape of the windings of a standard construction gasket to the form of an asymmetric shape – Fig. 1b. The effect of such a design was enhanced stiffness, as well as tightness of the gasket at low values of contact stress.

2 Problem formulation

Spiral wound gaskets based on PTFE have so far been the best and only solution applied in installations that store and transport the substances of acids. The main drawback of spiral wound gaskets with PTFE filling is their slight tightness at a small assembly contact stress (significantly smaller than that of a gasket based on EG). This is due to the smaller plasticity of PTFE in comparison with EG. Figure 2 includes the leakage characteristics of a spiral wound gasket with PTFE and EG fillings with inner and outer ring (IO).

As can be seen from Fig. 2, obtaining tightness of $1 \cdot 10^{-1}$ mg/(s·m), in the case of a spiral wound gasket DN40 PN40 with a PTFE filling embedded in the internal and external metal ring, requires stress of about 104,7 MPa. In the case of a gasket of the same size, but with EG

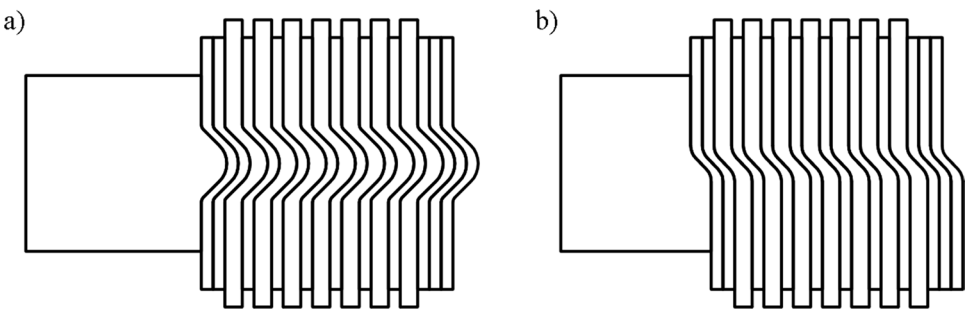

Fig. 1 Design of a spiral wound gasket **a** standard design, **b** asymmetric profile of windings

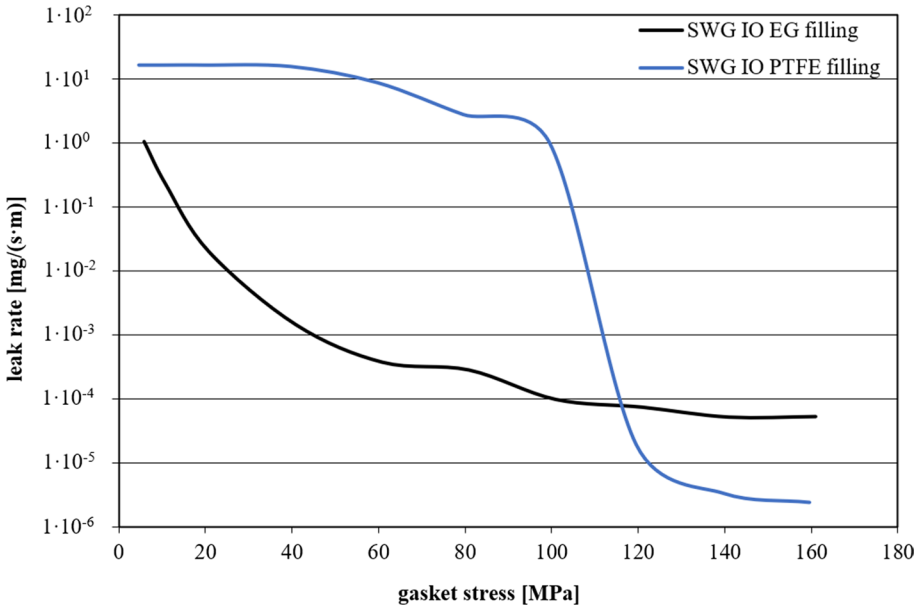

Fig. 2 Comparison of the tightness characteristics of a spiral wound gasket with PTFE and EG fillings

filling achieving such a leakage level, it requires stress of about 13,9 MPa. Only at a stress of about 116,1 MPa is the leakage from both gaskets within the same level, that is, $1{\cdot}10^{-4}$ mg/(s·m). A further increase in stress leads to an advantage of the PTFE filling over EG filling with regard to the tightness of the gasket. Nevertheless, in the case of very large gasket diameters, a guarantee of such a high contact stress value is sometimes impossible, and it generally causes the exceedance of the permissible stress of bolts and flanges [15].

Moreover, the excessive growth of the assembly load of bolts leads, among others, to the reduction of the effective width of the gasket, the decrease in local contact stress on the internal side of the gasket, as well as its excessive increase on the external side [16–18] or deformation and rotation of flanges [18]. Consequently, an excessive rotation of flanges leads to leakage growth and, in extreme cases, to the destruction of the gasket. In accordance with the ASME 16.20 standard [19], the optimal load of a spiral wound gasket in the assembly phase involves exerting the proper value of stress in the cross section of the bolt's root. In the case of gaskets measuring from 1/2, ¾, and '1,' and which have a pressure class of 150, 300, and 600, the stress should be equal to 172 MPa. For other measurements of gaskets, the stress should be equal to 207 MPa.

The purpose of the work was to develop a spiral wound gasket with an asymmetric profile of windings with PTFE filling, which solves the problem of low tightness and stiffness. Furthermore, with the use of numerical calculations, experimental research and the theory of fractals, the influence of the shape of the steel tape and the soft filling material on the operating parameters of the gasket was determined.

3 Mechanism of an SWG

A properly constructed gasket should, primarily, be characterized with low internal porosity and the ability to fill in the irregularities of the flanges' surfaces. These two essential features of gaskets result directly from the elimination of the potential leakage paths through which the gasketed medium tries to pass—Fig. 3. One of the paths is leakage via the internal gasket's structure. Therefore, a desirable feature is low porosity. Another path occurs on the contact surface of the gasket and the flange's face**.** Thus, the gasket material should be characterized with a high ability to fill in the irregularities of sealing surfaces (flanges), that is, possess big compressibility (plasticity). Soft materials such as EG and various kinds of rubbers undoubtfully have this second feature.

In a spiral wound gasket, the dominant leakage path is the one that occurs on the contact surface of the gasket and flanges' surfaces. Due to alternate interlacing of the metal tape with the elastic one, the leakage via the internal structure is totally eliminated. A problem (especially at low stress) occurs when there is leakage on the contact surface. A basic role in this case is played by the compressibility (plasticity) of the material filling the metal windings of the spiral. Figures 4 and 5 present a method that exemplifies a hypothetical mechanism of the deformation of a spiral wound gasket filled with an elastic material of high compressibility, such as EG (Fig. 4a–c), as well as a material of lower compressibility, such as PTFE (Fig. 5a–c). In the initial phase, both gaskets are in an unloaded state (Fig. 4a and Fig. 5a). Starting from the analysis of the deformation of the gasket shown in Fig. 4, it can be seen that a filling material of high compressibility fills in the irregularities of gasketed

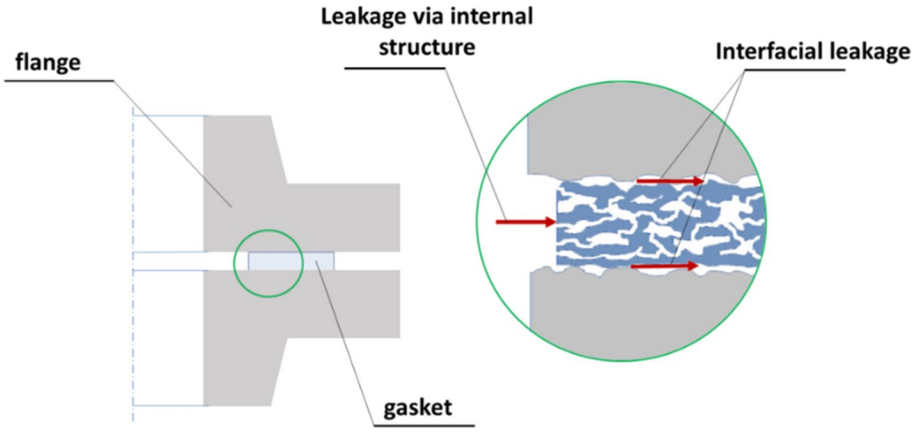

Fig. 3 Leakage paths from the gasketed flange-bolted joint

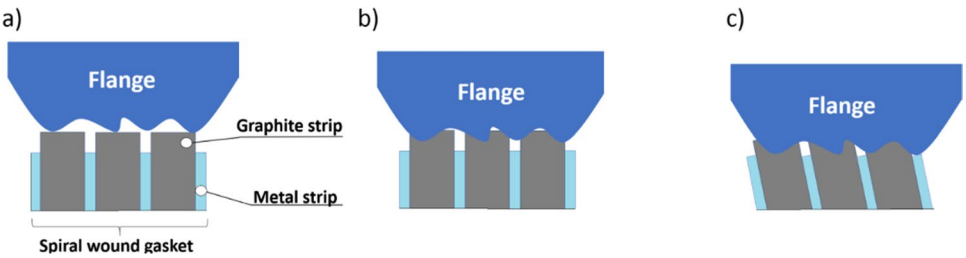

Fig. 4 Mechanism of a spiral wound gasket filled with EG

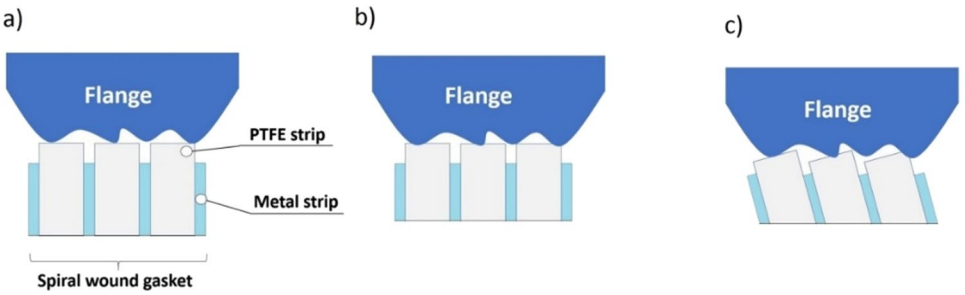

Fig. 5 Mechanism of a spiral wound gasket filled with PTFE

surfaces easily at slight compression (Fig. 4b). Since the cross section of the windings of the spiral is shaped in the form of the letter 'V,' a further increase of the axial deformation windings of the gasket causes simultaneous growth of the side deformation occurring in the direction of the internal diameter. As a result, the filling material and the windings of the metal tape gradually begin to lose their vertical position, inflecting toward the external diameter of the gasket—see Fig. 4c. Nonetheless, at such a state of deformation, the tape made of the high elasticity material still maintains a high degree of filling the irregularities of sealing surfaces.

The above-presented method of the deformation of the windings of filling material tape of great compressibility can serve as an explanation for the high tightness of the spiral gasket with a graphite filling at a low contact stress. When analyzing the behavior of the gasket filled with the material of lower compressibility (e.g., PTFE), it can be assumed that in the first load phase (Fig. 5b) a degree of filling the irregularities of the sealing surfaces may be a bit smaller than in the previous example. This results from the fact that PTFE has higher stiffness than EG.

Similarly, as in the earlier described example, along with the increase of the axial deformation of the gasket, there is a gradual inflection of the gasket's windings from the contact plane with the gasketed surfaces (Fig. 5c).

Consequently, there is a reduction of the contact surface of the windings of the filling material tape with sealing surfaces, the result of which is a reflection of smaller tightness. Only at a relatively large contact stress can the degree of filling the irregularities of the sealing surfaces with a PTFE material be comparable with the degree which is provided by EG. Therefore, at a bigger stress, both solutions present comparable leakage levels.

Transferring the above considerations to the possibility of increasing the tightness of the spiral wound gasket with a PTFE filling, it seems reasonable to construct such a gasket,

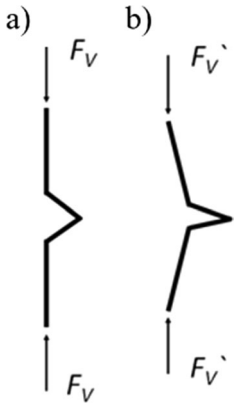

Fig. 6 Mode of deformation of the metal tape/coil of the standard gasket

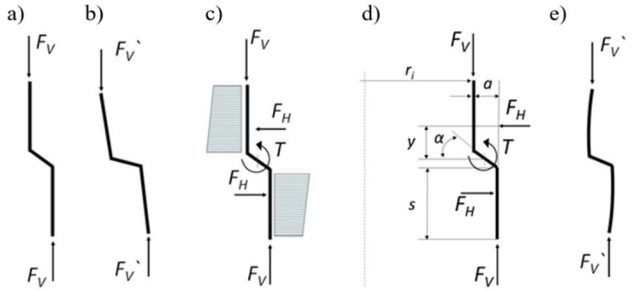

Fig. 7 Mode of deformation of the metal tape/coil of the asymmetric profile of windings

which when stressed, the windings of the metal and PTFE tapes would maintain a vertical position (the contact parallel with sealing surfaces) for as long as possible. In this way, the gasket would keep a constant contact surface, independent of the deformation level. A gasket with an asymmetric construction of the profile of windings, which is presented in Fig. 1b), can be characterized with such a feature.

4 New design of an SWG

As said in the previous paragraph, the result of the low tightness of the spiral wound gasket with PTFE filling is the untimely loss of the steadiness of the vertical segments of the windings, which as a result leads to the lowering of the contact surface of the filling material tape with sealing surfaces. While analyzing the way of deformation of a single coil of the tape of the standard construction gasket—Fig. 6a, it can be stated that when subjected to force (*Fv*), the coil in question will deform to the form presented in Fig. 6b.

It is worth underlining that on such a type of single element of the coil, friction force additionally acts, which herein has been omitted. In the case when a single segment of the coil took an asymmetric shape (Fig. 7a), the coil, which is hypothetically subjected to force (*Fv*), would then deform to the shape presented in Fig. 7b. However, such a shape of a single segment causes the action of a pair of force F_V on the arm a, which consequently evokes torque T equal to:

$$T = F_V \cdot a \tag{1}$$

This torque, on the other hand, causes a pair of force F_H transversely directed to the vertical part of a segment—Fig. 7c:

$$F_H = \frac{T}{y} \tag{2}$$

where a—arm of acting force F_V, y—arm of acting force F_H

Assuming that there is a trapezoidal distribution of contact stress on the side vertical area of segments, the arm of acting force F_H is:

$$y = \frac{a}{2}\sin\alpha + \frac{1}{3}s \tag{3}$$

Finally, the deformation of the metal tape will take the form similar to the one presented in Fig. 7d.

The mean value of stress acting on the vertical segment of the tape can be shown as:

$$p = \frac{F_H}{A_V} = \frac{F_V \cdot a}{\frac{a}{2}t\sin\alpha + \frac{1}{3}s} \cdot \frac{1}{2\pi \cdot r_i \cdot s} = \frac{F_V \cdot a}{\pi \cdot r_i\left(a\sin\alpha \cdot s + 2/3 s^2\right)} \tag{4}$$

where F_H—horizontal force, F_V—vertical force, a—arm of acting vertical force, $A_V = 2\pi \cdot r_i \cdot s$—side area on which force F_H acts, s—length of vertical metal coil's segment, r_i: diameter i-of the coil's segment

$$r_i = n \bullet t + r_1 \tag{5}$$

$$t = t_s + t_g \tag{6}$$

where n—number of segments (metal windings), t_s— thickness of the metal coil, t_g—thickness of the coil of the filling tape, r_1—diameter of the internal spiral.

At such a deformation arrangement of a single coil of the tape, the effect of maintaining the PTFE segment in a vertical position is more probable. Additionally, a new design of spiral wound gasket can exhibit higher resistance against the axial thrust, since during the axial deformation the vertical segments of the asymmetric windings are less prone to deform in radial direction in relation to symmetric windings. Furthermore, due to the diagonal position of the middle element of the tape's profile, this construction still allows big elasticity to be maintained.

5 Experimental research

5.1 Research subject

The subject of experimental research involved two constructions of a spiral wound gasket with PTFE filling embedded in the internal distance ring. The first design was a standard gasket, which is presented in Fig. 1a. The second solution was a non-standard design, characterized by the asymmetric shape of the windings' cross section— Fig. 1b. The constructions of both solutions were based on the nominal dimensions of the gasket with the designation of PN40 DN40, which is compliant with the EN-PN 1514-2 standard [20]. The equivalent of this solution is the 2″ class 600 gasket, which is in accordance with the ASME 16.20 standard [19]. In the assumed constructions, the metal distance ring was made of steel 1.4301 with a thickness of 3 mm. The spiral part of the gasket was made of metal tape with a thickness of 0.18 mm, and PTFE tape with a thickness of 0.3 mm. On each spiral there were 9 coils of the PTFE tape and 13 coils of the metal tape, whereby the beginning and end of the spiral consisted of three metal coils, respectively. As a result, the following measurements of gaskets were obtained: internal diameter of the metal ring $d_1 = 50$ mm, internal diameter of the spiral $d_2 = 56$ mm, external diameter of the spiral $d_3 = 68$ mm, and total height of the gasket $h = 5.5$ mm.

5.2 Test rig

Figure 8 presents the test rig in which the main element was a hydraulic press with a maximum force of 1 MN. The press was equipped with detectors for registering displacement and force. Additional elements of the test rig included a helium detector and a set of pressure gauge used to determine leakage by means of the differential method. The arrangement of the elements of the test rig was controlled by a computer and, depending on requirements, it could simulate the work of the gasket in conditions similar to those in a flange-bolted joint.

5.3 Research procedure

The experimental research was conducted in order to obtain the elastic behavior, tightness level, and the creep-relaxation ratio of the two gaskets' construction.

5.3.1 Test procedure concerning stiffness characteristic

The sequence of such a procedure was as follows. After measuring the dimensions, the gasket was placed on the lower plate of the hydraulic press, and then, the upper plate of the press was moved closer with minimum stress. Next, an automatic procedure in a controlling program was turned on. Its aim was to gradually load the gasket with stress in the range from 0 to 100 MPa. After reaching the targeted stress value, the controlling program gradually lessened the stress until the final value of 5 MPa. The rate of stress change at the load, as well as at the unload of the gasket, was 0.5 MPa/s. At the same time, along with the change of load, the program registered an axial deformation of the gasket, which consequently allowed the relation between contact stress and the compression set to be determined.

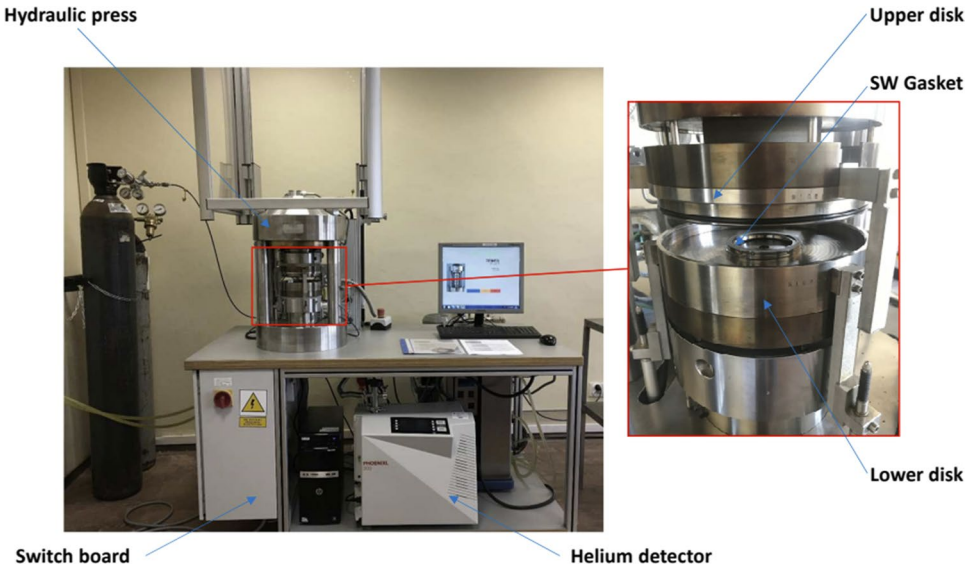

Fig. 8 Test rig

5.3.2 Test procedure concerning the leakage characteristics

After measuring the dimensions and placing the gasket on the lower plate of the press, the gasket was gradually loaded in eleven steps with stress in the range from 5 to 40 MPa. The change of stress was also made by the controlling program. In each determined stress point, helium of pressure equal to 40 bar was added to the inside of the gasket and the leakage level was measured for 10 min. The registration of the stress value and the corresponding measured leakage value allowed the determination of the so-called tightness characteristics.

5.3.3 Test procedure concerning creep-relaxation

This procedure (as the two mentioned above) started with measuring the gaskets' dimensions. Next, the gasket was placed in the lower plate of the press and clamped to the upper plate. The initial gasket's contact stress was set to 40 MPa. The lower and upper plates were then heated to the required temperature. In this test, the gaskets were tested at 100 °C.

The heating rate of the plates was 1.5 °C/min. After reaching the required temperature, the gaskets' thickness, as well as contact pressure, was registered over the course of 4 h.

5.4 Tests results

5.4.1 Stiffness characteristics

Figure 9 presents the record of dependence of the contact stress acting on the surface of the gasket in the axial compression function of the two tested gaskets. In the initial range of load, i.e., from 0 to 100 MPa, the course of the relation between stress and deformation is similar. The similarity results from the fact that only fragments of the windings of the PTFE tape that protrude above the windings of the metal tape underwent a big deformation in this load range. At a stress value of 40 MPa, the asymmetric gasket deformed by 0.6 mm, while the standard gasket deformed by 0.8 mm. Significant differences in the deformations of both solutions can already be seen at a stress of 60 MPa, where for the asymmetric gasket the deformation value was noted on the level of 0.65 mm, and for the standard one it was 1.6 mm. At the maximum stress of 100 MPa, the deformation in the asymmetric gasket was 1.6 mm, and in the standard one, it was 2.3 mm. The unload curves of both solutions are basically parallel to each other. Nonetheless, the plastic deformation at stress reduction to 5 MPa in the asymmetric gasket was 1.5 mm, and in the standard one, it was 2.1 mm.

5.4.2 Tightness characteristics

Figure 10 shows the characteristics determining the leakage level from the gaskets in the function of the exerted gasket contact stress. In the stress range from 5 to 15 MPa, both gasket constructions show a very high leakage level, falling within the range of $1 \cdot 10^2$ mg/(s·m). Along with the increase in load, the tightness level of the standard construction slightly improves, while in the asymmetric gasket, there is a significant change of the leakage reduction.

At the stress of 30 MPa, the leakage level of the standard gasket is about $2 \cdot 10^1$ mg/(s·m), and for the asymmetric gasket, it is $8 \cdot 10^0$ mg/(s·m). At the stress of 40 MPa, the leakage values differ by an order of magnitude. In the case of the

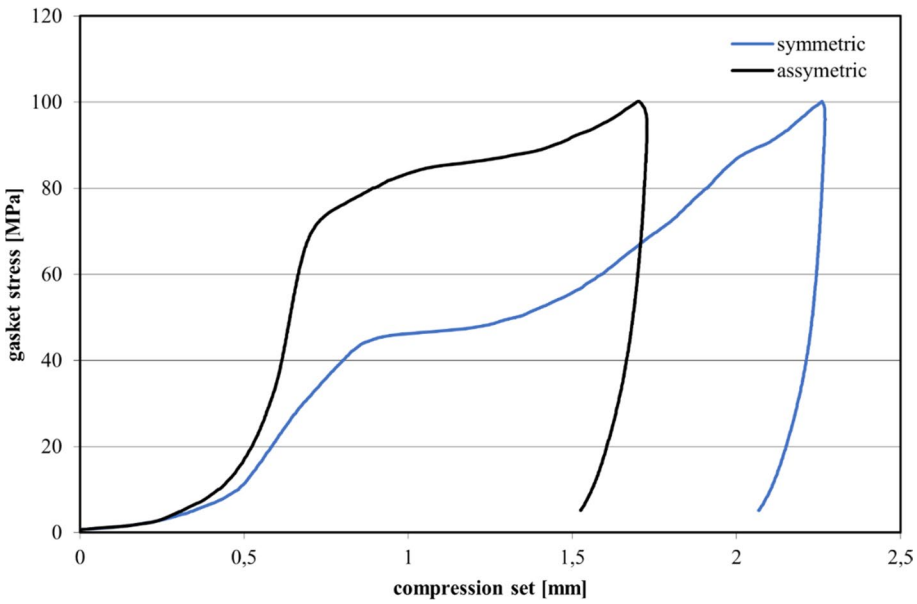

Fig. 9 Stiffness characteristics of both gaskets

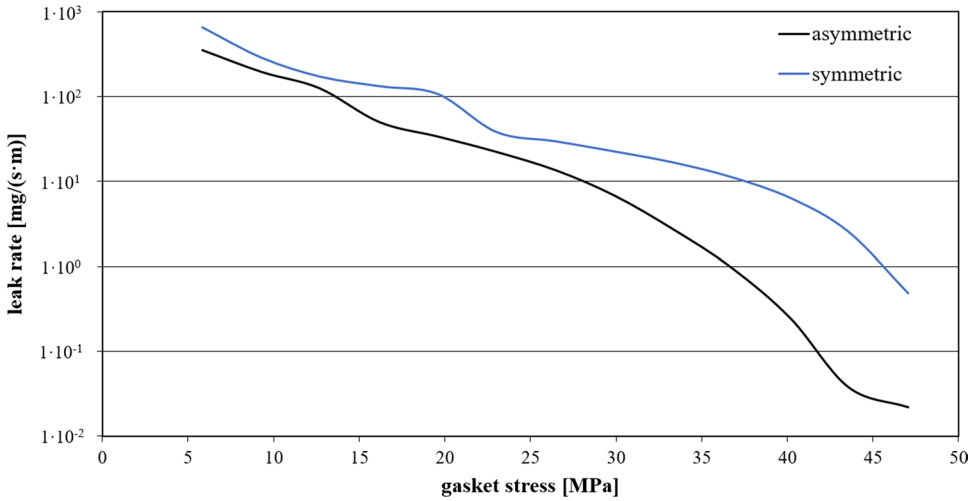

Fig. 10 Tightness characteristics of both gaskets

standard construction, the leakage was $7 \cdot 10^{0}$ mg/(s·m), and in the asymmetric one, it was $3 \cdot 10^{-1}$ mg/(s·m).

5.4.3 Creep-relaxation

Figure 11 presents the relationship between the contact stress vs the compression set of the two gasket constructions subjected to a temperature of 100 °C.

Based on this figure, it can be seen that the compression level of the standard gasket, under a contact pressure of 40 MPa, is significantly larger than in the case where the gasket is operated at ambient temperature. At ambient temperature, the compression set of this gasket was 0.8 mm (see Fig. 9), while at 100 °C the compression was nearly 1.2 mm. In the case of the asymmetric gasket, its compression both at ambient and elevated temperatures did not change. At the contact stress of 40 MPa, the compression set at ambient and elevated temperatures was nearly the same and equal to 0.6 mm. The most important parameter, which derives from the characteristics presented in Fig. 11, is the creep-relaxation ratio. Its graphic representation is shown in Fig. 12 (based on the characteristics of the asymmetric gasket). This ratio is defined as the final contact pressure (after 4 h of testing) over the initial contact pressure (in this test it was 40 MPa):

$$P_{\mathrm{QR}} = \frac{\sigma_{(4h)}}{\sigma_0} \tag{7}$$

where $\sigma_{(4\ \mathrm{h})}$—final contact pressure, σ_0—initial contact pressure.

For the standard and asymmetric gaskets, the value of the creep-relaxation ratio was 0.79 and 0.88, respectively. It is worth mentioning that this kind of test does not consider the additional effect that can have a major influence on creep-relaxation level. This effect is the bolts' relaxation. Therefore, later in the article, the authors described the tests that were performed for both gaskets operating in a flange bolted

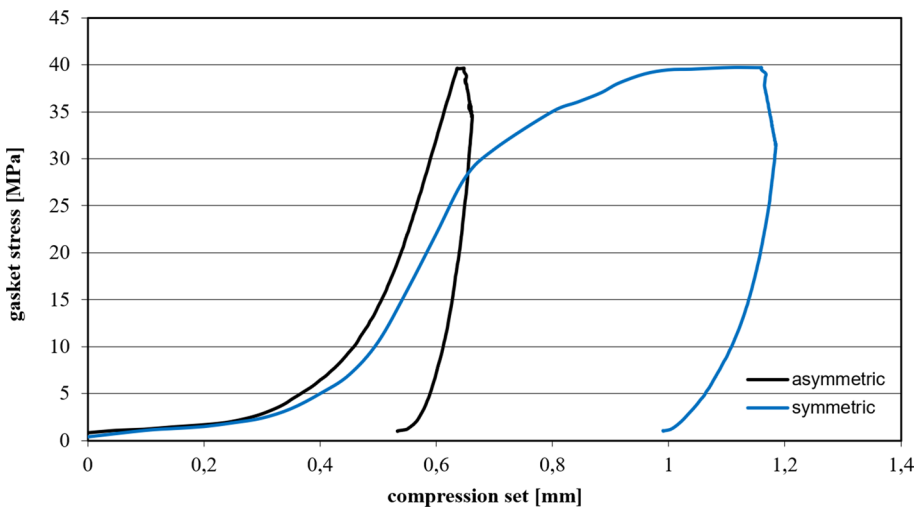

Fig. 11 Relationship between the contact pressure vs the compression set of the two gasket constructions subjected to a temperature of 100 °C

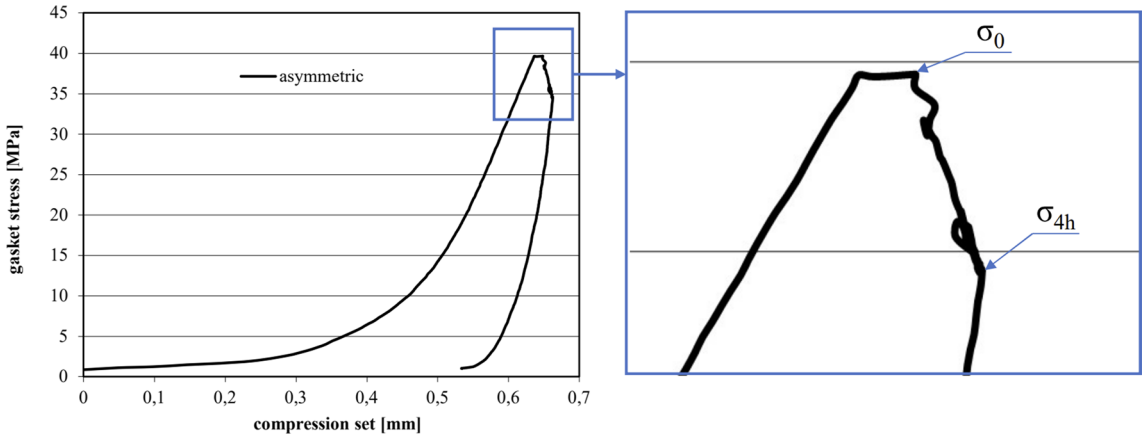

Fig. 12 Graphical presentation of the contact stress value included in Eq. (7)

joint and which were subjected to elevated temperature and internal pressure.

6 Numerical analysis

In order to confirm the considerations adopted in paragraphs 3 and 4 regarding the way in which the windings of the gasket deform, and also to determine the stress on the contact surface of the gaskets' windings, numerical analysis was conducted. It was based on the finite element method using the ANSYS Workbench R22 utility static structural analysis.

6.1 Numerical model

The numerical model was built as axisymmetric in two configurations, that is, a gasket with a standard shape of windings, as well as a gasket with an asymmetric shape of windings. Discretization of the area of particular parts was made using finite elements of higher order. The 8-node quadrilateral planar elements were chosen. The average size of finite elements in area of spiral windings was 0.05 mm. The average size of elements 0.08 mm and 0.3 mm were set up for metal rings and plates, respectively. The mesh in such figuration includes 42,000 elements and 134,000 nodes. A division into finite elements and boundary conditions is presented in Fig. 13. The top and bottom plates of the hydraulic press, as well as the metal windings and the internal ring of the gasket, were modeled with an isotropic, bilinear steel material with the following parameters: Young modulus $E = 200{,}000$ MPa, Poisson's ratio $v = 0.3$, module of strengthening in the plastic deformation zone $E_U = 8000$ MPa, yield stress $Re = 240$ MPa. The windings of the PTFE were modeled with an isotropic, bilinear material with the following parameters: Young modulus $E = 310$ MPa, Re = 11 MPa,

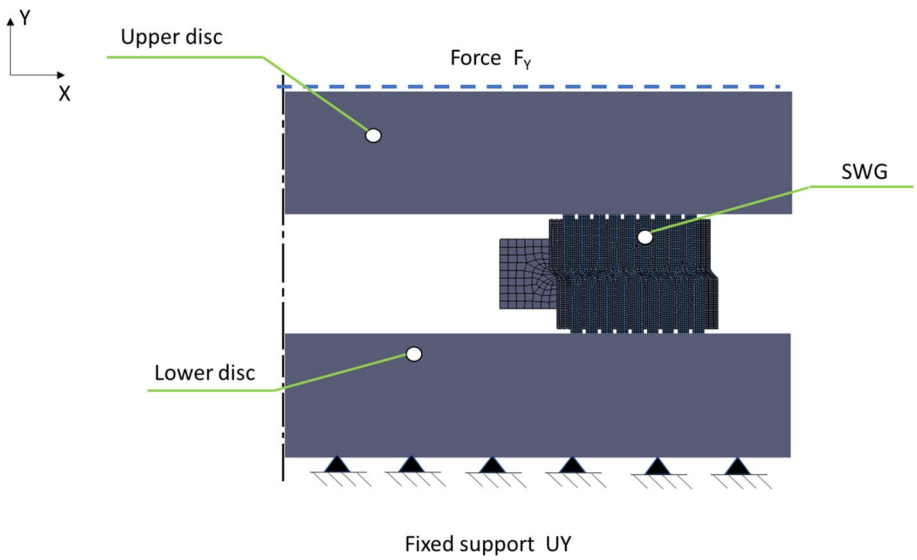

Fig. 13 Numerical model of the spiral gasket

strengthening modulus $E_U = 10.5$ MPa, and Poisson's ratio $v = 0.42$. The straitening modulus defined in bilinear material model represents the ratio between stress and strain in a plastic zone. The characteristic of the PTFE material model is presented in Fig. 14. On the contact area of the metal tape with the press's plates, a friction contact with a coefficient of 0.16 was set. This is a typical value of friction coefficient for non-lubricated metal-to-metal contact. The friction coefficient between PTFE and metal tapes/platens was set as 0.05, this value was taken from reference [21]. The lower plate of the hydraulic press was fixed. In the upper plate, the value of force causing a stress of 40 MPa was $F = 46.7$ kN, which corresponded to the nominal contact surface of the gasket.

The analysis was conducted with an active function of nonlinearity of materials and the possibility of large deformation. The issue of convergence was solved using the Newton–Raphson method. It should be noted that providing larger deformations (larger stress) in a simulation of this type of construction brings about the problem of gaining convergence of numerical results, that is, the nonlinearity of the material, nonlinearity of the deformation, and nonlinearity of the contact (friction).

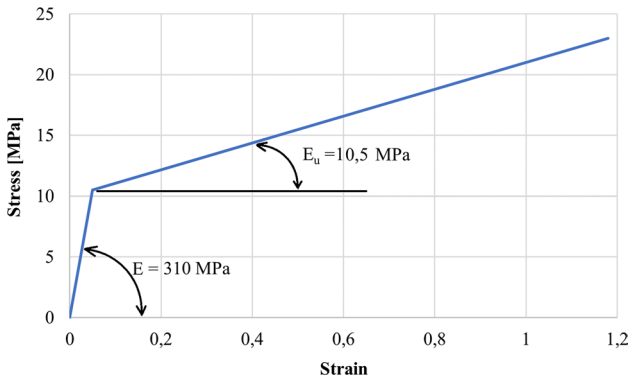

Fig. 14 Characteristics of the PTFE model

6.2 Calculation results

Figure 15 presents a map of equivalent stress (according to von-Mises hypothesis) in the PTFE tape of both constructions of gaskets at a compression to stress of 40 MPa, which corresponds to the maximum value at which the tightness level was determined.

In the case of the standard gasket**,** the maximum stress in the PTFE tape appeared in two areas, that is, at the contact of the PTFE tape with the metal plate, and in the rounded part of the tape in the middle part of the profile 'V.' At the stress of 40 MPa, the gasket deformed axially by 0.72 mm. It can also be noticed that the deformation of the PTFE tape confirms the effect of the angular deflection (presented in Fig. 5) of the windings of the PTFE tape from the contact plane with sealing surfaces.

In the case of the asymmetric gasket, the distribution of stress in the contact area was more regular. At the given load, the gasket deformed axially by 0.58 mm. The maximum stress in this case occurred at the contact surface of the PTFE tape with the plates. Moreover, it can be observed that the vertical segments of the PTFE tape maintained their vertical position at the given load. For a better comparison of both constructions, Fig. 16 presents the stress distribution in the contact area of the PTFE tape with the plates of the hydraulic press. Figure 16a clearly shows the irregularity of the distribution of the contact pressure on the PTFE tape in the standard solution of the gasket. In turn, Fig. 16b shows a more regular distribution. The regularity of the distribution of contact stress and the larger area of contact leads to the enhancement of the tightness level in this solution of gasket.

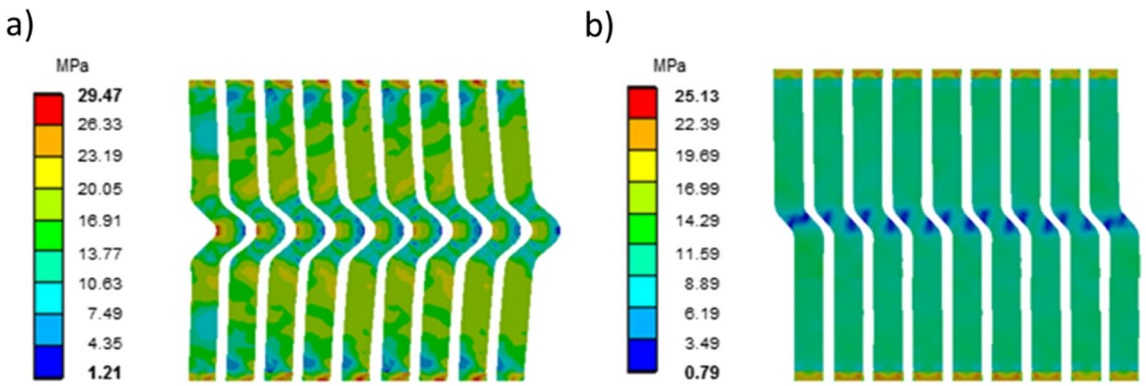

Fig. 15 Distribution of stress in the PTFE tape, **a** symmetric windings, **b** asymmetric windings

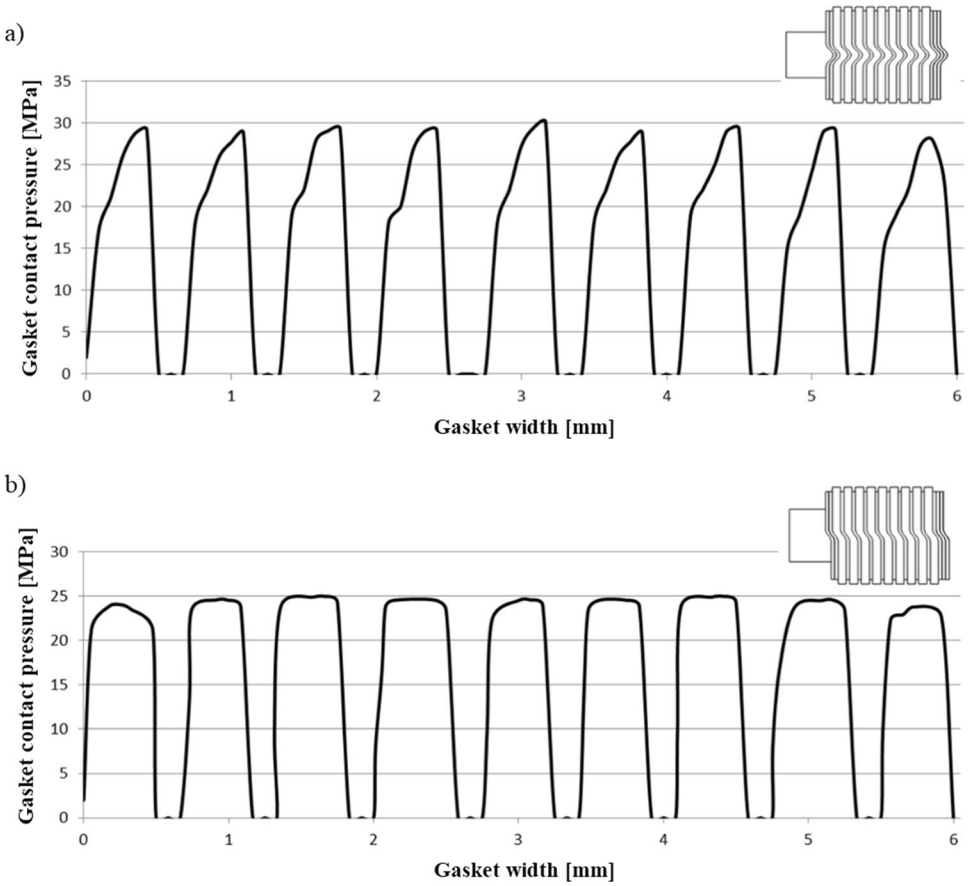

Fig. 16 Distribution of stress on the segments of the PTFE tape; **a** symmetrical windings, **b** asymmetrical windings

7 Topographic analysis of the contact surface

In this paragraph, the analysis of the topography of the contact surfaces of the two gasket constructions was performed. The investigation was performed on gaskets subjected to 100 MPa stress. The analysis was made by means of the laser technique, using the Olympus OLS5000 microscope. A contactless measurement enabled a very exact scanning of the whole plane in 3 dimensions, where the diagonal resolution was as high as 0.12 µm. Due to the fact that the gasket recovers elastically after unloading, the profile of the contact surface determined by this method does not fully reflect the windings' arrangement that occurred at the time of contact with the plates of the hydraulic press. Figure 17a presents the image of the contact surface of the asymmetric gasket.

Based on this photo, an image of the surface topography was made (Fig. 17b), and then, the profile (Fig. 17c) was determined. The course of the profile clearly shows that an asymmetric profile maintains the parallelism of the contact surface of the PTFE tape in a very good degree. The same method as above was used to take a picture of the surface, as well as to determine the contact profile of the standard gasket—Fig. 18.

The image of the map presented in Fig. 18b clearly shows that the windings of the PTFE tape lost the parallelism of the contact surface. This effect manifests itself in the form of a very irregular profile, which exactly shows the angular inflection of the windings of the PTFE tape. Pictures of the cross sections of both constructions can be found in Fig. 19. Figure 19a, which presents the asymmetric arrangement of windings, proves that only one side of the gasket maintains more vertical positions of the windings at such great stress (100 MPa). The windings on the opposite side lost parallelism. Therefore, at a larger stress, the tightness of this solution might not be as diverse (compared to the standard construction), as it takes place in the stress range from 10 to 40 MPa. Hence, a conclusion can be made that the asymmetric gasket increases tightness at a smaller contact stress. However, in the range up to 100 MPa, the stiffness of this solution improves significantly, which can be seen in the chart in Fig. 9.

8 Qualitative comparison of the two gaskets design

As mentioned in paragraph 5.4.3, the dominant leakage component in the case of the spiral wound gasket is the one occurring in the contact surfaces. If these surfaces are

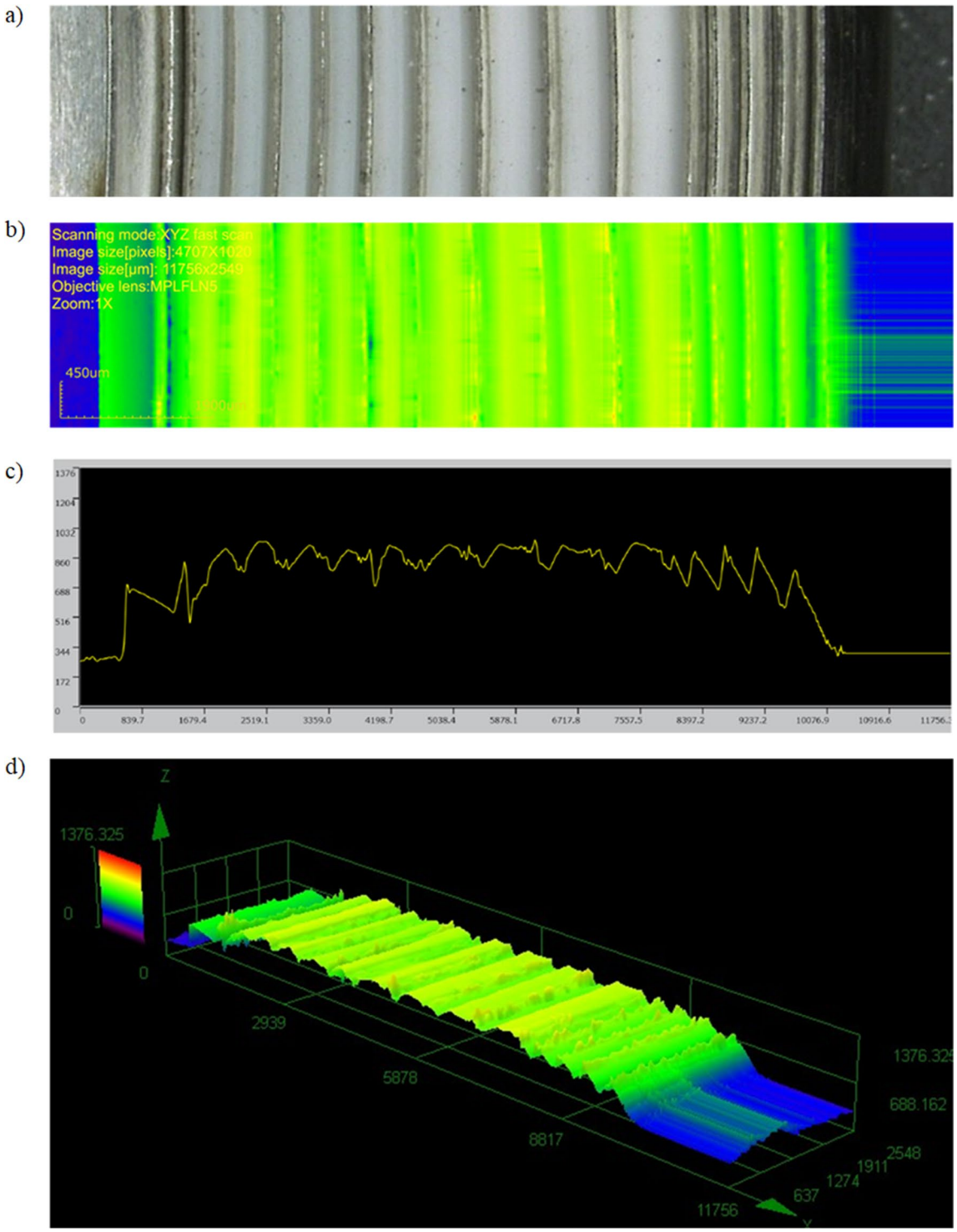

Fig. 17 Pictures of the topography of the asymmetric gasket's contact surface

too harsh and strongly irregular, the leakage level is a more intensive. Obviously, when the contact pressure increases, the leakage decreases. Nonetheless, as presented in work [16, 18], the leakage level from the interfacial sealing surface does not only depend on the magnitude of the contact pressure. In addition, the most important factors that have an influence on the leakage are: the distribution of the contact pressure and the effective contact area. As proved in papers [17, 18], if the gasket construction provides a more regular contact pressure distribution along the gasket's width, the

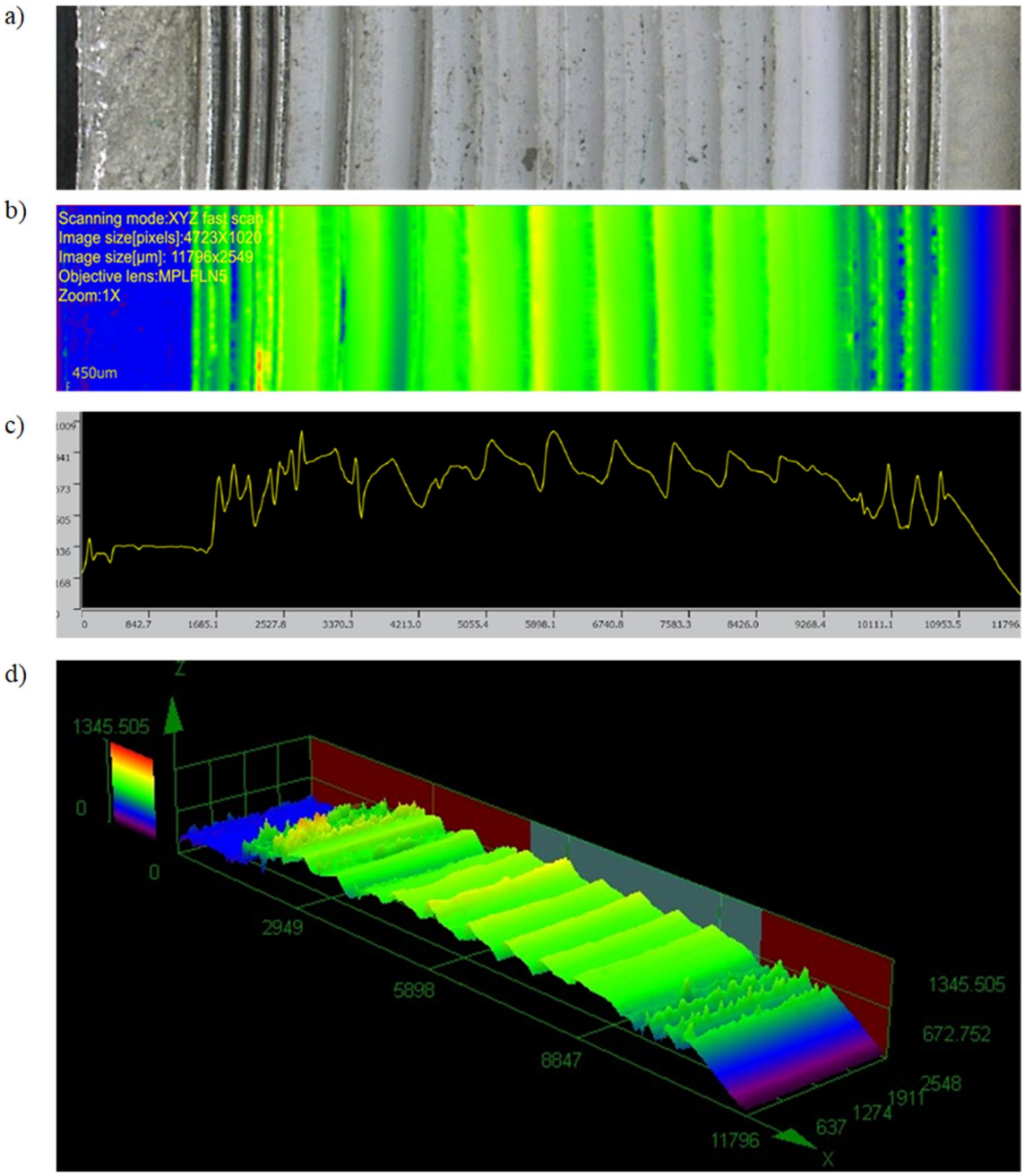

Fig. 18 Pictures of the topography of the standard gasket's contact surface

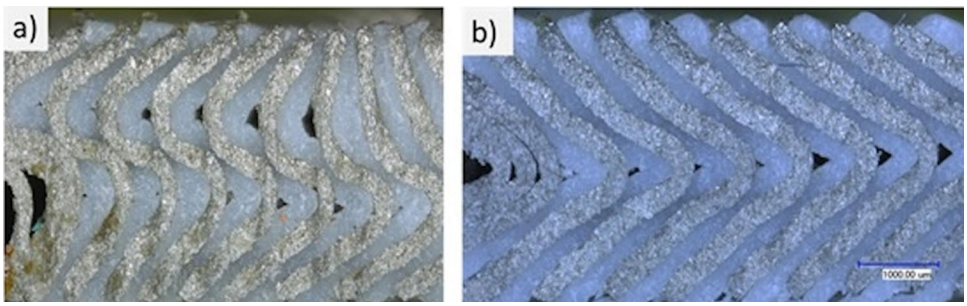

Fig. 19 The gaskets' profiles at a stress of 100 MPa; **a** asymmetric gasket, **b** symmetric gasket

leakage level is smaller than that in a gasket in which the contact pressure was higher but concentrated only in a small region. The effective contact area is a factor that is strictly related to the roughness of the sealing surface. Vast research concerning the influence of roughness and hardness on the leakage level from sealing surfaces was presented in papers. [22–26]In these papers, fractal theory was used to determine the basic parameters responsible for leakage. One of them is the permeability of contacting surfaces. Using the equation presented in [22], the permeability of contacting surfaces can be expressed by the formula:

$$K_v = \frac{\pi D_f \lambda_{\max}^4}{128\tau\left(4 - D_f\right)S} \tag{8}$$

where $\lambda_{\max}$—maximum capillary diameter,D_f—the fractal dimension of tortuous capillaries, τ—the capillary's tortuosity, S- cross section.

Permeability is the one of the basic components included in the Darcy formula describing the leakage rate of a porous structure in the form of a ring subjected to internal pressure:

$$Q = \frac{2\pi K_v f(p_o - p_t)}{\mu \ln\left(\frac{r_t}{r_o}\right)} \tag{9}$$

where f—the height of the vertical direction of the percolation channels, p_o, p_t—the internal and external pressure, respectively, μ—the fluid viscosity, r_o, r_t—the internal and external radius of the ring.

Based on formulas (8) and (9), it can be seen that apart from the parameters of the fluid, such as viscosity and pressure, the leakage level strongly depends on the micro-geometry of the sealing surface, especially the maximum diameter of the pore $\lambda_{\max}$. It is a parameter that has a major influence on the leakage intensity, since its value, in accordance with Eq. (8), is to the power of four.

On the other hand, the maximum diameter of the pore is strictly connected with the topography of the sealing surface [22]:

$$\lambda_{\max} = f\left(S_{\max,p}; l_{\max,p}\right) \tag{10}$$

where $S_{\max,p}$—the maximum cross section of a pore:

$$S_{\max,p} = G^{D-2}(\ln\gamma)^{1/2} l_{\max,p}^{(4-D)} \tag{11}$$

$l_{\max,p}$—the maximum length of a pore:

$$l_{\max,p} = \sqrt{\left[\frac{4(3-D)A_t}{\pi(D-1)} - l_{\max}^2\right]} \tag{12}$$

Other parameters included in formulas (11) and (12) are:

G—roughness constant, D—the fractal dimension of the pores, γ—frequency spectrum,A_t—the apparent area of seal-contact interface, $l_{\max}$—the maximum length of an asperity.

In accordance with research data presented in paper [24], the quality of the leakage proofness of the two rough contacting surfaces can be described by two fractal parameters. The former is the fractal dimension of the pores D, and the latter is the roughness constant G. If the fractal dimension of the pores tends to its maximal value 2, and the roughness parameter tends to the minimum value, the sealing surfaces exhibit high leakage proofness.

In this paragraph, the parameters D and G were used in order to explain why the asymmetric gasket exhibits better leakage proofness than the standard gasket. These parameters can be determined from the profiles obtained from the topography analysis presented in paragraph 7. In Fig. 20, the characteristic fractal geometries of two gasket surfaces were presented. The length and peak of the characteristic and maximum asperity can be directly read from the analyzed section of the profile. To determine the fractal dimension of the pore, the circles method was used. This method is the equivalent of the box-counting method presented in paper [25].

This method involved inscribing circles of various sizes that represent the diameter of the i-th capillaries into the empty areas of the sealing surface profile. In accordance with Eq. (13), the pore area fractal dimension D can be determined by the value of the slope of the linear fitting of data on a logarithmic plot of the cumulative number of pores N_i versus the pore size λ_i.

$$N(L \geq \lambda) = \left(\frac{\lambda_{\max}}{\lambda}\right)^D \tag{13}$$

These relationships, in the form of a chart for both the gaskets (standard and asymmetric), are presented in Fig. 21.

In the case of the asymmetric gasket, the fractal dimension of the pores was $D = 1.86$, whereas for the standard gasket, it was $D = 1.482$. The roughness constant G was calculated using formula:

$$G = \sqrt[(D-2)]{\frac{\delta}{2(\ln\gamma)^{1/2} l^{(3-D)}}} \tag{14}$$

where δ—the characteristic peak of asperity, l—the characteristic length of asperity both taken from the profiles presented in Fig. 20.

The characteristic parameters describing the fractal geometry of both profiles are collected in Table 1. For the asymmetric gasket, the roughness parameter was $G = 5.34 \cdot 10^{-7}$, and for the standard gasket, it was $G = 1.54 \cdot 10^{-4}$. Based on parameters D and G, it can be concluded that the asymmetric gasket exhibits a better quality of sealing surface than standard gasket. This effect was achieved thanks to the fact

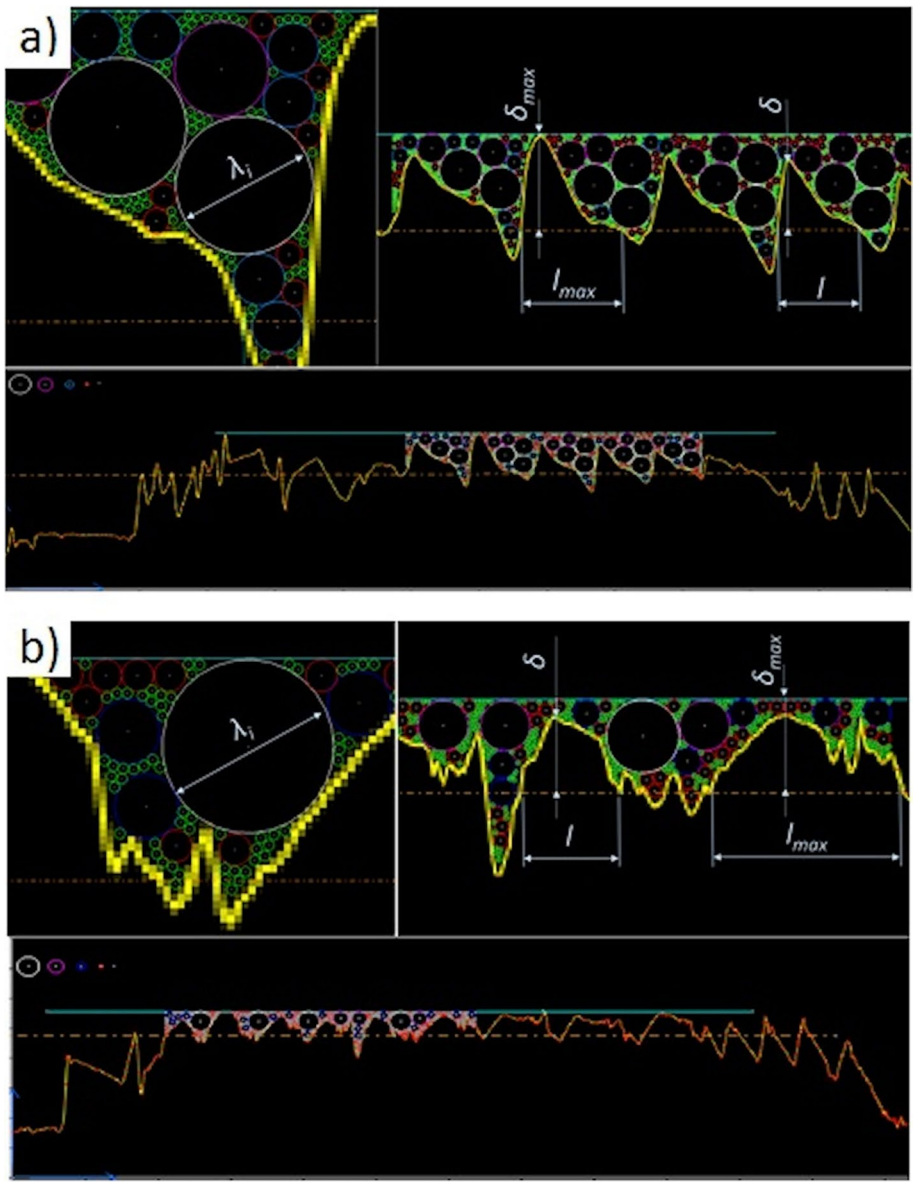

Fig. 20 Characteristic fractal geometry of the two gasket surfaces **a** symmetric gasket, **b** asymmetric gasket

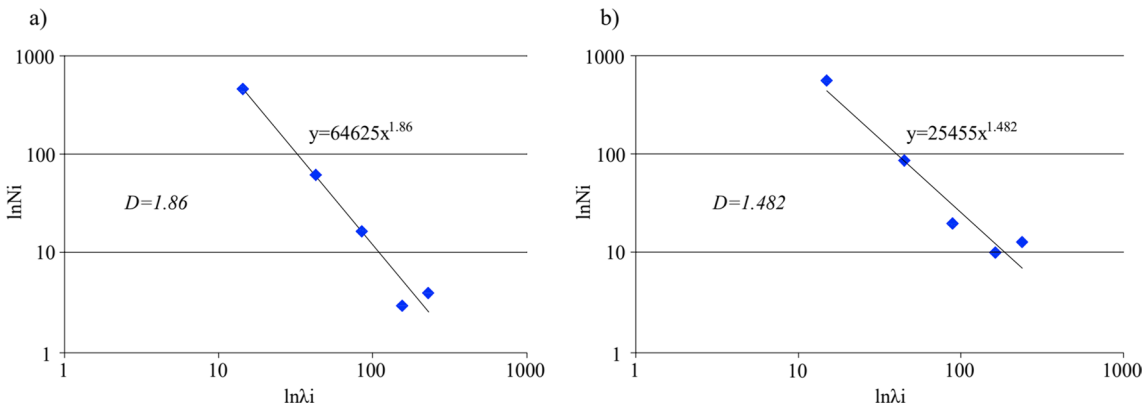

Fig. 21 A logarithmic plot of the cumulative pore number $N(L > \lambda)$ versus λ_i. **a** asymmetric gasket, **b** standard gasket

Table 1 Characteristic parameters describing the fractal geometry of the gaskets' profile

Gasket profile	δ µm	l µm	δ_{max} µm	l_{max} µm	D-	G-
Asymmetric	237	247	242	771	1.860	$5.34 \cdot 10^{-7}$
Standard	387	512	415	691	1.482	$1.54 \cdot 10^{-4}$

that the winding structure did not deform too excessively under gasket compression, and that the upper PTFE segments stayed in vertical positions, which provided a better adhesion to the flange's sealing surface. The D and G parameters constitute only a qualitative comparison of the two solutions of the gasket construction.

Quantitative determining of the leakage according to Eq. (9) requires a more detailed description of the fractal structure of the sealing surface profile, but this task is outside the scope of this work.

9 Conclusions

On the basis of the conducted experimental research and numerical calculations, the following conclusions can be drawn:

- The asymmetric gasket exhibits larger stiffness when compared to the gasket with a standard construction. At a contact stress of 100 MPa, the gasket with an asymmetric profile deforms by 1.6 mm, while the standard one deforms by 2.3 mm.
- Based on the tightness test, it was found that in the range of stress from 5 to 40 MPa, the asymmetric gasket exhibits higher tightness in comparison with the standard one. At a contact stress of 40 MPa, the difference in the leakage value is more than an order of magnitude. At this contact stress, the leakage from the asymmetric gasket is
- $3 \cdot 10^{-1}$ mg/(s·m), while the leakage from the standard gasket is $7 \cdot 10^{0}$ mg/(s·m).
- The numerical analysis of the gaskets' compression proved that stress distribution on the contact surface of the gasket with the asymmetric shape is more regular than for the standard gasket.
- This relationship was also proved in the topography analysis, where it was evidenced that at the same level of axial load the windings of the standard gasket deformed more excessively. Nevertheless, at larger stress values (above 40 MPa), the effect of maintaining the parallelism of contact becomes gradually lost. The vertical windings of the gasket begin to deform excessively, as evidenced in the cross section pictures taken at the stress of 100 MPa.
- Based on qualitative analysis of both gaskets' sealing surface, it was found that under compression the surface of the standard gasket deformed more than in the case of the asymmetric gasket. The main factors that allowed the gaskets' surface quality to be assessed were the basic fractal parameters in the form of the fractal dimension of the pores—D, and the roughness constant—G. For the asymmetric gasket, these parameters were equal to $D = 1.86$, $G = 5.34 \cdot 10^{-7}$, whereas for the standard gasket, it was $D = 1.482$, $G = 1.54 \cdot 10^{-4}$.

Acknowledgements Calculations have been carried out using resources provided by Wroclaw Centre for Networking and Supercomputing (http://wcss.pl), grant No. 444.

Declarations

Conflict of interest The authors whose names are listed immediately below certify that they have NO affiliations with or involvement in any organization or entity with any financial interest (such as honoraria; educational grants; participation in speakers' bureaus; membership, employment, consultancies, stock ownership, or other equity interest; and expert testimony or patent-licensing arrangements), or non-financial interest (such as personal or professional relationships, affiliations, knowledge or beliefs) in the subject matter or materials discussed in this manuscript. I have no conflict of interest to disclose.

References

1. Winter JR, Leon GF (1985) Radially inward buckling of spiral wound gaskets. american society of mechanical engineers. Press Vessels Pip Div PVP-Vol 98:111–116
2. Larson RA, Bibel G (2005) Experimental and analytical evaluation of buckling forces of a spiral wound flexible gasket. Proc ASME Press Vessels Pip Conf Comput Technol PVP-vol 2:97–104
3. Mueller RT (1996) Recent buckling experiences with spiral wound flexible graphite filled gaskets. American Society of Mechanical Engineers, Pressure Vessels and Piping Division PVP-Vol. 326, Computer Technology- Applications and Methodology: 23–34
4. Jaszak P, Walencki Ł (2018) Testing of the gaskets at liquid nitrogen and ambient temperature. Open Eng 8:329–336

5. Celzard A, Mareche JF, Furdin G (2003) Describing the properties of compressed expanded graphite through power laws. J Phys Condens Matter 15:7213–7226
6. Fanasov IM, Savchenko DV, Ionov SG, Rusakov DA, Seleznev AN, Avdeev VV (2009) Thermal conductivity and mechanical properties of expanded graphite. Inorg Mater 45(5):486–490
7. Zhang Z, Wang D, Guo Y (2019) Fretting friction and wear behaviors of spiral wound gasket (SWG) sealing surface. Tribol Int 133:236–245
8. Dowell MB, Howard RA (1986) Tensile and compressive properties of flexible graphite foils. Carbon 24(3):311–323
9. Nunes LCS, Dias FWR, da Costa MHS (2011) Mechanical behavior of polytetrafluoroethylene in tensile loading under different strain rates. Polym Test 30:791–796
10. Goyal RK, Yadav M (2013) Study on wear and friction behavior of graphite flake-filled PTFE composites. J Appl Polym Sci 127:3186–3191
11. Shibo W, Li P, Li P (2013) Tribological behaviors of polytetrafluoroethylene composites under dry sliding and seawater lubrication. J Appl Polym Sci 130:2523–2531
12. Xue Q, Zhang Z, Liu W, Shen W (1998) Friction and wear characteristics of fiber- and whisker-reinforced PTFE composites under oil lubricated conditions. J Appl Polym Sci 69:1393–1402
13. Zhang Z, Liu W, Xue Q, Shen W (1997) Friction and wear characteristics of PTFE composites filled with metal oxides under lubrication by oil. J Appl Polym Sci 66:85–93
14. Zhang Z, Xue Q, Liu W, Shen W (1998) Friction and wear characteristics of copper and its compound-filled PTFE composites under oil-lubricated conditions. J Appl Polym Sci 70:1455–1464
15. Jaszak P, Adamek K (2019) Design and analysis of the flange-bolted joint with respect to required tightness and strength. Open Eng 9:338–349
16. Feng X, Gu BQ, Liu R (2006) Finite element analysis for the metallic gasket effective width. Comput Methods Eng Sci 21–23:232–232
17. Jaszak P (2019) The elastic serrated gasket of the flange bolted joints. Int J Press Vessels Pip 176:103954
18. Jaszak P (2019) A new solution of the semi-metallic gasket increasing tightness level. Open Eng 9:329–337
19. ASME B16.20 (2017) Metallic gaskets for pipe flanges. American Society of Mechanical Engineers, New York
20. EN 1514-2 (2021) Flanges and their joints—Gaskets for PN-designated flanges—part 2: spiral wound gaskets for use with steel flanges
21. EN 1591-1 Annex E (2014) Flanges and their joints—design rules for gasketed circular flange connections—part 1: calculation method
22. Zhang Q, Chen X, Huang Y, Chen Y (2018) Fractal modeling of fluidic leakage through metal sealing surfaces. AIP Adv 8:045310
23. Zheng Q, Xu J, Yang B, Yu B (2013) A fractal model for gaseous leak rates through contact surfaces under non-isothermal condition. Appl Therm Eng 52:54–61
24. Zhang Q, Chen X, Huang Y, Zhang X (2018) An experimental study of the leakage mechanism in static seals. Appl Sci 8:1404
25. Yu B, Cheng P (2002) A fractal permeability model for bi-dispersed porous media. Int J Heat Mass Transf 45:2983–2993
26. Pérez-Ràfols F, Larsson R, Almqvist A (2016) Modelling of leakage on metal-to-metal seals. Tribol Int 94:421–427